Journal of
Materials Chemistry B

Accepted Manuscript

This is an *Accepted Manuscript*, which has been through the RSC Publishing peer review process and has been accepted for publication.

Accepted Manuscripts are published online shortly after acceptance, which is prior to technical editing, formatting and proof reading. This free service from RSC Publishing allows authors to make their results available to the community, in citable form, before publication of the edited article. This *Accepted Manuscript* will be replaced by the edited and formatted *Advance Article* as soon as this is available.

To cite this manuscript please use its permanent Digital Object Identifier (DOI®), which is identical for all formats of publication.

More information about *Accepted Manuscripts* can be found in the **Information for Authors**.

Please note that technical editing may introduce minor changes to the text and/or graphics contained in the manuscript submitted by the author(s) which may alter content, and that the standard **Terms & Conditions** and the **ethical guidelines** that apply to the journal are still applicable. In no event shall the RSC be held responsible for any errors or omissions in these *Accepted Manuscript* manuscripts or any consequences arising from the use of any information contained in them.

Journal of Materials Chemistry B RSCPublishing

ARTICLE

The effect of self-assembled fibers on the synthesis, characteristics and biomedical applications of CCAG hydrogels

Xian Li, Daidi Fan*, Chenhui Zhu, Xiaoxuan Ma

Cite this: DOI: 10.1039/x0xx00000x

Received 00th November 2013,
Accepted 00th 2013

DOI: 10.1039/x0xx00000x

www.rsc.org/

CS-HLC-HA/β-GP (chitosan-human-like collagen-hyaluronic acid/β-sodium glycerophosphate) hydrogels were prepared based on the self-assembly of CS-HLC-HA (CCA) fibers. The effects of the fibers on the synthesis, characteristics and biomedical applications of CS-HLC-HA/β-GP (CCAG) hydrogels were studied for various HA contents. The synthesis mechanism of the novel CCAG hydrogel was explored using Fourier transform infrared spectroscopy (FT-IR) and X-ray photoelectron spectroscopy (XPS). The hydrogels were characterized by a swelling test, gelling time and enzymatic treatments. The results indicated that a new amide bond (-CONH) and $-NRH_2^+$ were formed. The gelling time and swelling behaviors were dependent on the intertwining, overlap and adsorption of the polymer chains at various temperatures and pH. Furthermore, biomedical applications were evaluated by transmission electron microscopy (TEM), immunohistochemical analysis and haematoxylin and eosin (H&E) staining. The effect of the fibers on the histocompatibility of the hydrogels revealed that the fibers inside the hydrogel pores reduced the quantity of macrophages, decreased the degree of inflammation, and improved the anti-degradation of the modified hydrogels. This type of new hydrogels emerges as an interesting injectable filling biomaterial for tissue engineering.

Keywords: Fibers; Hydrogels; Self-assemble system; Histocompatibility; issue engineering

Introduction

Self-assembling systems that are mainly used in enzymes, proteins and DNA have emerged as potential candidates for the development of safe nanostructured scaffolds in tissue engineering and biological sciences.[1] Knowledge of the rules of intermolecular association, the so-called bottom-up approach, facilitates the design of molecular assemblies such as membranes, films, layers and gels for biomedical applications.[2, 3] Increased attention has been currently paid to the layer-by-layer (LBL) self-assembly technique via crosslinking to form hydrogels, for which the driving force is based on the consecutive adsorption of polyanions and polycations via electrostatic interaction, hydrogen bonding interaction, hydrophobic interaction or specific biological interaction between biomolecules.[4] It is a versatile, inexpensive yet efficient technique to "build" biologically active surfaces made of both synthetic and natural polymers in biomaterials.[5-7]

Hydrogels derived from natural polysaccharides are ideal scaffolds.[8] These hydrogels vary in terms of the overall charge, hydrophobicity and type of polar amino acids, resulting in nonstructured fibrillar networks with various swelling ratios and gelling times. For a natural hydrogel made of self-assembled peptides, each peptide has a critical minimum concentration for forming clear solid-like hydrogels in water. With an increased peptide concentration, the gel changes its appearance from clear to translucent to opaque white and exhibits increased rigidity.

The self-assembled film infiltrates and covers the hydrogel surface and then affects its physicochemical properties.[9] Self-assembled hydrogels may contain macroscopic structures such as fibers that are entangled with each other and form meshes. The fibers can be assembled through the repetitive and direct adsorption of components of opposite functionalities. However, it is also difficult to produce an injectable and biodegradable hydrogel[10] using the layer-by-layer self-assembly technique because of the body environmental and physiological condition considerations of biomedical applications. Therefore, using the self-assembly technique to form the fibers and using the fibers to fabricate the hydrogel using a cross-linking agent would overcome the rapid degradation of the hydrogel and affect the properties of the hydrogels including their elasticity, swelling

ratio, surface morphology and appearance and then improving the biological activities of the hydrogels *in vivo*.

Natural polysaccharides such as hyaluronic acid (HA, hyaluronan) have been extensively studied in medical applications because they not only provide intrinsic biological activities but also regulate the differentiation of endodermal stem cells[11] and deliver stable proteins.[12] For chitosan/hyaluronan (CH/HA) multi-layered films, Richert et al.[13] demonstrated that there was a decrease in cell adhesion with an increase in the layer number. This result occurred because the increased layer number resulted in a more uniform and smooth surface, while a rougher film offered a large surface area for cell attachment.[13]

Recent studies reported that HLC has been used in hydrogel[14], artificial bone[15-17] and vascular scaffolds[18] due to its water solubility, poor rejection, workability, good biocompatibility, biodegradability and no risk of viral infection. Costa et al.[19] reported the layer-by-layer assembly of chitosan and recombinant biopolymers into biomimetic coatings, which have considerable stimuli-responsive properties. Because of its good biocompatibility, biodegradability, antibacterial and wound-healing property, chitosan is formulated in various forms including powders, films,[20] beads,[21] hydrogels[22,23] as well as porous scaffolds.[24] The feasibility for the preparation of some of these derivatives together with their enhanced biomedical properties, which are useful especially in the areas of tissue engineering, is an exciting prospect.[25]

In this study, our objective is to develop CCAG hydrogels containing fibers (CS-HLC/HA) that are entangled with each other and form meshes in β-GP solution. Here, β-GP was applied as the cross-linking agent for the formation of hydrogels. The CS-HLC/HA fibers were formed using the self-assembly technique, which may have the potential to produce a hydrogel with novel properties including improved biocompatibility, anti-biodegradability and anti-inflammatory properties. An additional study was performed that investigated the process and mechanism of the *in-vitro* and *in-vivo* degradation. The results demonstrated that the novel CCAG hydrogel would be suitable for soft tissue filling.

Materials and Methods

Materials

HLC was expressed by *E. coli* with a cloning partial cDNA derived from human collagen Mrna.[26] It is a macromolecular water-soluble protein with a molecular weight of 97,000 (China patent number: ZL01106757.8). HA (molecular weight, 1,000,000) was purchased by Shandong Frieda Biological Technology Limited Company (China). Chitosan (molecular weight, 550,000; 90-92% deacetylation) was obtained by Qingdao Ocean Ltd. Co. (China). All the other solvents and reagents were analytical grade.

Preparation of CS/HA films

Chitosan was dissolved in 0.1 mol/L acetic acid (HAc) aqueous solution with a concentration of 5% (w/v) and placed in a 10-mL centrifuge tube. HA solutions with concentrations of 2%, 1%, 0.5% and 0.1% were prepared with distilled water. The HA solution was added into the CS solution at a volume ratio of CS and HA of 5:1. The film was removed and rinsed repeatedly in distilled water until becoming clear. The sample was then dried under vacuum. The film was examined by scanning electron microscopy (SEM).

Preparation of CS-HLC/HA fibers

The CS-HLC/HA fibers were prepared by mixing 5% (w/v) chitosan dissolved in 0.1 mol/L acetic acid (HAc) aqueous solution with an isocratic volume of 3% (w/v) human-like collagen aqueous solution. The mixture was stirred for 20 min in an ice-water bath until dissolution was complete. Then, HA solutions with various concentrations (2%, 1%, 0.5% and 0.1%) were added at a volume ratio of CS: HLC: HA of 5:5:1. The mixture was then stirred until fibers were formed in the solution by self-assembly. The CS-HLC/HA (CCA) solution was poured into the Petri dish and dried under vacuum. The sample was examined by phase-contrast imaging and scanning electron microscopy (SEM).

Preparation of the CCAG hydrogel

The pH/temperature-sensitive CCAG hydrogels were prepared by mixing the CS-HLC/HA (CCA) solution with 1 mL 40% β-GP and stirred for 20 min in an ice-water bath until dissolution was complete and the pH of the sol solution reached 7.4 (see Table 1). The solutions were then placed in a thermo cell for gelling at various temperatures.

FT-IR spectroscopic analysis

FT-IR spectra were recorded using a Nicolet FT-IR 5700 spectrophotometer (Thermo Fisher Scientific, Waltham, MA, USA) at ambient conditions. The characterization of the four components (CS, HLC, HA and β-GP) and CCAG hydrogel samples were triturated with KBr at a ratio of 1:100 and pressed to form pelleted samples for FT-IR spectroscopic analysis at 500-4000 cm^{-1}.

X-ray photoelectron spectroscopy (XPS)

X-ray photoelectron spectroscopy (XPS; Thermo Fisher, ESCALAB 250Xi, USA) was used to determine the elemental composition of the CCAG hydrogels, in which full (pass energy, 100 eV) and high-resolution spectra (pass energy, 20 eV) were recorded.

Measuring gelling times

The gelling time was determined using the tube inverting method[27, 28] using a 10-mL centrifugal tube. Approximately 2-4 mL of sol was placed in the centrifugal tube and inserted in a thermo cell until the solutions stopped flowing (Fig. 3 A-B). The time lapsed during this process was recorded as the gelling time.

Table 1. The CCAG hydrogel composition.

Sample	CS (mL)[a]	HLC (%)	HA (%)	β-GP (mL)[b]
Gel1	2	3	2	1
Gel2	2	3	1	1
Gel3	2	3	0.5	1
Gel4	2	3	0.1	1

[a] CS is 5 wt.% aqueous solution.

[b] β-GP is 40 wt.% aqueous solution.

Swelling measurement

For the temperature/pH-dependent swelling studies, dried gels were placed in triplicate in physiological saline and PBS buffer solutions with pH values of 5, 7.4 and 9 at various temperatures for at least 24 h to reach equilibrium, after which the gels were weighed. The classical gravimetric method was employed to measure the swelling ratio of the hydrogels. The equilibrium swelling ratio was given as $(W_s-W_d)/W_s$, where W_s and W_d represent the weight of swollen gel and the dried gel, respectively.

Microscopic investigations

The pore morphology of the CCAG hydrogels before and after degradation was examined by scanning electron microscopy (SEM). The samples (Gel1, Gel2, Gel3 and Gel4) were carefully lyophilized to maintain their three-dimensional porous structures (without any collapse) before and after degradation. The lyophilized hydrogel samples were immersed in liquid nitrogen, and the vitrified samples were carefully cut with a cold knife. The cut samples (cross-sections and vertical-sections of the hydrogels without degradation and cross-sections of hydrogels after degradation by enzyme) were mounted, sputter-coated with gold, and observed under SEM using a Hitachi S-570 SEM microscope (Hitachi, Tokyo, Japan).

***In vitro* degradation**

Degradation of hydrogels was performed *in vitro* using Collagenase I (0.5 mg/mL), Hyaluronidase (HAse) (100U/mL) and Trypsin (100U/mL). The dried samples were weighed and sterilized by Co^{60} irradiation and then immersed in tubes containing 5 mL of fresh enzyme solution. The tubes were kept static at 37.0 ± 0.5℃ in a cell culture box. After soaking for 1, 2, 3, 4, 5 or 6 weeks, the samples were withdrawn from the enzyme solution and then rinsed with ultrapure water for 30 min for three times. After lyophilization, the dry weights were measured. The weight loss (W_L) was calculated according to $W_L= (W_0-W_1)/W_0\times100\%$, where W_0 and W_1 are the weights of the sample before and after soaking, respectively. This process was applied to three parallel samples, and the mean value of the weight loss rate was calculated.

***In vivo* histocompatibility evaluation**

1. Injection of hydrogels

Assessment of the *in vivo* biocompatibility of hydrogels was performed by injecting the sol into male Kunming mice (20–25 g). After shaving and disinfection, 0.2 mL of the sol was injected subcutaneously into the back of the Kunming mice. Before treatment, all the animals were quarantined for a week, allowing free access to food and water but not any antibiotics.

2. Transmission electron microscopy (TEM) analysis

The population of 45 Kunming mice was divided into five groups: the negative control group was injected with physiological saline, while the others were injected with Gel1, Gel2, Gel3 and Gel4. After anesthesia with methoxyflurane, a 0.2-mL sample of the relevant hydrogel was injected subcutaneously into the dorsal midline. The injected tissue was removed 1 day, 14 days or 48 days post-surgery. Tissue blocks of 1 mm^3 were fixed immediately with 2.5% phosphate-buffered glutaraldehyde (GA) for 2 h, rinsed with 0.1M PBS for 30 min, post-fixed in 1% osmium tetroxide for 2 h, and finally rinsed for 10 min using a 0.1 M phosphate buffer. The samples were then dehydrated using an ethanol series (30, 50 and 70%) for 10 min at each concentration and stained in 70% ethanol solution of uranyl acetate for 2 h. Next, the samples were dehydrated with 90% ethanol (2, 3 and 10 min) and then 100% ethanol (3, 3 and 10 min), displaced by epoxyethane. Finally, the samples were embedded in Epon 812. Semi-thin sections (1–2 μm) were cut and stained with methylthioninium chloride to select appropriate areas for observation. Ultrathin sections (50–70 nm) were stained with 4% uranyl acetate and 0.5% lead citrate and observed under TEM (HITACHI, H-600, Japan). Three samples for each group were used for the TEM analysis.

3. H&E staining and Immunohistochemical analysis

In this analysis, 0.2 mL of the sol was injected subcutaneously into the back of the Kunming mice. After 1, 2 or 6 weeks, the mice were sacrificed, and the tissue surrounding the hydrogels was removed and immediately fixed in 10% neutral buffered formalin. The tissue was then dehydrated through a graded ethanol series, immersed in liquid wax and then embedded in epoxy resin. Blocks were sectioned using a Leica RM2016 diamond saw microtome (Leica Instruments Ltd, Germany) with a blade thickness of 5 mm and collected on coated slides. Half of the sections were prepared for histopathological analysis using haematoxylin and eosin (H&E) staining, and the other half was used for immunohistochemical analysis. For the H&E staining, the sections were processed through a series of ethanol dehydrating and embedded in paraffin. Sections (5 μm)

were cut and stained with haematoxylin and eosin (H&E) for tissue observation using a light microscope (Nikon eclipse 80i, Japan). For the immunohistochemical analysis, the population of 45 Kunming mice was divided into five groups; the control block involved staining by CD68 without anti-CD68 mAb 1 week after injection with Gel1, Gel2, Gel3 and Gel4, while the others involved staining by CD68 with anti-CD68 mAb 1, 2 and 6 weeks after injection with Gel1, Gel2, Gel3 and Gel4. The primary antibody used was CD68 (Santa Cruz Biotechnology, US). The sections were incubated in HRP-labeled second Abs (Sigma Aldrich, US) for 30 min in a humidified 37℃ chamber. The sections were then rinsed three times in PBS and incubated in a 4% diaminobenzadine substrate solution at room temperature. Images were acquired using a light microscope (Nikon eclipse 80i, Japan).

Calculations and data analysis

The data were collected in a Microsoft Excel 2000 database, and the results were presented as the means and standard deviations using the Origins 7.0 software. A Student's t-test was performed to determine the statistical significance between experimental groups. A value of $p < 0.05$ was considered to be statistically significant.

Results and discussion

FI-IR spectroscopic analysis

The differences in chemical structures between the CS, HA, HLC, β-GP and CS–HLC–HA/β-GP (CCAG) determined by FT-IR are presented in Fig. 1. In the spectrum of the CS–HLC–HA/β-GP hydrogel (CCAG), new characteristic peaks (–RNH_2^+) at 2625 cm^{-1} and 1619 cm^{-1} were formed mainly due to the conjugation of P atoms on $–OPO_3^{2-}$ with N atoms from –NH_3^+ (Scheme. 1E), which represents the stretching vibration of V_{NH2+} and the bending vibration of δ_{NH2+}. The characteristic peaks representing the stretching vibration of V_{C-N} were observed at 1413 cm^{-1}, in reverse, which were absent in HA, CS and HLC and was consistent with the formation of -CONH at -C=O sites on HLC coordinated with -NH_2 sites on CS in CS/HLC or -NH_2^+ of CS being reacted with the $–COO^-$ of HA, the fibers formed with an amide bond (-RCONHR'). This result is mainly due to β-GP as the crosslinking agent playing an important role in the synthesis of the hydrogel. The characteristic peaks representing the stretching vibration of $V_{C=O}$ decreased from 1644 cm^{-1} to 1619 cm^{-1}. This result indicates that CS, HLC, HA and β-GP underwent intermolecular interactions during the gelation process and possibly produced a hydrogen bond and decreased the stretching vibration frequency of C=O, while the final composition of these four monomers did not participate in the reaction completely. However, compared with pure HLC, pure CS and pure HA, the characteristic peaks of V_{OH} and V_{C-O} in the CCAG hydrogels undergo no significant changes. Compared with the CCG hydrogel[29], there is a significant difference between the fibers formed by the self-assembly technique and the other controls with the HA-added CCAG hydrogels.

XPS analysis

Table 2. Assignments of main specials bands based on their binding energy for the CCAG hydrogel composition.

Element	HLC/eV	CS/eV	HA/eV	β-GP/eV	CCAG/eV	Assignments
C 1s	284.79	284.85	284.76	284.84	284.6	C-C
C 1s	286.2	286.25	286.27	286.29	286.2	C-N, C-O C-O-C
C 1s	287.85	287.79	287.72	---	287.85	C=O O-C-O
N 1s	399.83	399.78	399.38	---	399.83	NH_2
N 1s	---	---	---	---	399.31	NH_2^+
P2p3	---	---	---	132.62	132.72	P=O
P2p1	---	---	---	133.57	133.49	P-OH P-ONa

XPS is mainly used for the qualitative analysis of surface elements and elemental valences. As observed in Fig. 2, all five types of polymers composed of the pure HLC, pure CS, pure HA, pure β-GP or CCAG hydrogel exhibited significant differences in all six peaks: C1s (284.0-285.0 eV), C1s(286.0-287.0 eV), C1s(287.0-288.0 eV), N1s (399.0-400.0 eV), P2p1 (133-134 eV) and P2p3 (132-133 eV) in their XPS spectra (see Table 2). For the XPS spectra of nitrogen, the binding energy was decreased from 399.38 eV in HA to 399.31 eV in the CCAG hydrogel. This result is mainly due to the amide bond of HA being easy to hydrolyze in acidic conditions and the functional group -NH-C=O in HA transforming into -NH_2 or -NH_3^+. The electronegativity of C=O was greater than H such that the binding energy of nitrogen was decreased. However, the binding energy of nitrogen was increased from 399.78 eV in CS to 399.83 eV in the CCAG hydrogel. This result is mainly due to the amide bond being consistent with the formation of -CONH at -C=O sites on HLC coordinated with -NH_2 sites on CS in CS/HLC or -NH_3^+ of CS being reacted with the -COO^- of HA. The fibers formed an amide bond such that the electronegativity of -C=O was greater than H, leading to the binding energy of -NH in CS being increased. Because the electronegativity of -OH was greater than -NH, the binding energy of C=O was decreased from 287.85 eV in HLC to 287.77 eV in the CCAG hydrogel, and the binding energy of C-N was decreased from 286.25 eV in CS to 286.01 eV in the CCAG hydrogel. Therefore, based on Fig. 1 and Fig. 2, a new amide bond (-CONH) and -NRH_2^+ were formed.

In addition, the binding energy of C-O was decreased from 286.27 eV in HA to 286.01 eV in the CCAG hydrogel. The XPS spectra peaks of phosphorus (binding energy: 133.72 eV, 133.49eV) were observed for the CCAG hydrogel. Compared with β-GP, the binding energy of P=O was increased from

132.62 eV in β-GP to 132.72 eV in the CCAG hydrogel, which is mainly due to P=O in β-GP providing the unoccupied orbital and the -NH_3^+ in HLC or HA providing an electron, forming -NH_2^+---P=O (see Scheme. 1). Therefore, the electronegativity of P=O was increased, and the binding energy was increased.

Irreversibility of films-fibrous chains-hydrogels transition

The CS/HA film, the CS-HLC/HA fibrous chains and the CCAG hydrogel are shown in Fig. 3 (A, B), Fig. 3 (C, D) and Fig. 3 (E, F), respectively. The interface of the film became smoother and more transparent, which may be attributed to the electrostatic attraction dominating the adsorption of HA to CS. HA is usually considered an anionic polysaccharide, and CS is usually considered a polycationic macromolecule. Evidently, the electrostatic attraction dominates the adsorption of HA to CS.[30, 31] Wu et al.[32] reported that the mixing of 2% CS and 0.2% HA at a volume ratio lower than 1:0.1 resulted in a smoother surface, homogeneous features, good biocompatibility and good miscibility at the nanometer scale. Therefore, at a constant volume ratio of 5:1, HA a solution with various concentrations (2%, 1%, 0.5% and 0.1%) was mixed with 5% CS. The CS/HA fibers initially formed a thin film between the interface of CS and HA by layer-by-layer self-assembly. Then, the thickness of the film was increased with the increased HA volume (Fig. 4A). The film was removed and rinsed repeatedly in distilled water until it became clear (Fig. 4B). The film was entangled, resulting in the layered film, and the number of layers was increased with the increased concentration of HA, especially for 2% HA mixing with 5% CS (Fig. 4B).

The hydrogel maintains its sol state at room temperature while changing to a gel at body temperature. No matter how much the temperature decreases or increases, the gel maintain its shape initially, which is required for tissue engineering, especially for plastic surgery. The irreversibility of the hydrogel not only avoids sol flow into other skin positions but also is necessary to improve safety. To further understand the CCAG sol-gel transition, the sol and gel were observed after sol immersion in an incubator at 37℃ for 10-30 min, as described previously[33]. The sol (Fig. 4C) appeared as a transparent liquid with a small amount of fibers inside the bulk of the hydrogel due to its interaction with the HLC, HA and CS linked by peptide bonds (Scheme. 1E). It has been previously established that the inverted test tube method can be used to measure the gel formation[33] (see Fig. 4D). The jelly-like hydrogel is bright white and flexible, and it has a uniform pore size on its surface (Fig. 4G).

Due to the HA being completely recovered from the contaminant proteins, [31] instead of using co-precipitation, self-assembly was employed to prepare the CS-HLC/HA composite. Therefore, the structures of the CS-HLC/HA fibrous chains were changed completely, which is mainly ascribed to HLC playing an important role in the electrostatic attraction and constructing the main frame in the structure. At a constant volume ratio of 5:5:1, the composite of 5% CS and 3% HLC mixed with 0.5% of HA resulted in fibrous chains, as observed in Fig. 3 (C, D). The fibrous chains exhibited regular, clear, and especially thicker straight chains, while some thin bending chains crisscrossed and circled the straight chains. With the concentration of 0.1% HA in CCA solution, a single fibrous chain was observed by phase-contrast imaging. The fibers exhibited a dendritic structure (Fig. 4E). We also noted that when maintaining the reaction time and increasing the concentration of HA (0.5%), the thickness of the fibers was increased significantly (Fig. 4F). We observed that further assembly resulted in fibers. Some salts were separated out and appeared as white spheres. In Fig. 4H, fiber chains adsorbed and intertwined with each other, and surface sections exhibited homogenous chains throughout the entire film surface. Fig. 3C presents a model of the formation process of the CCA fibrous chains, where a single fibrous chain was composed of a CS chain, HLC chain and HA chain. From Figs. 3B, C and Fig. 4 E, F, H, HLC is the main-chain, CS is the sub-chain, and HA is the branched-chain in the dendritic structure (Fig. 4I). Thus, the SEM images supported the previous results obtained using the model of CCA chains, for which the formation process transitioned from a single fibrous chain to double fibrous chains interwound with each other to aggregated fibrous chains (Fig. 3G). Thus, the observed inverse correlation of hydrogel compatibility with HA concentration was expected.

In Fig. 4L, the CCAG hydrogel formation process via the self-assembly method using the CCA polymer (Scheme. 1D) immersed in β-Gp solution at body temperature is shown. Compared with CS-HLC/HA fibrous chains, the structure of the CCAG hydrogels changed from an irregular and unclearly interior structure to a homogeneous and clearly interior network structure. The unique structure is useful for transferring the water and body fluids to the filling positions. Therefore, the self-assembled film transformed into self-assemble fibers and hydrogels mainly due to β-Gp playing an important role as a crosslinking agent, and the fibrous internal structures, introduction of HA, and positively charged chitosan in the fibers may provide more space for water and allow small molecules to move freely in the network. Therefore, for CCAG hydrogels, the sol-gel transition was irreversible.

Gelling time dependence on temperature

Fig. 4M shows the effect of the HA concentration on the gelling time of the hydrogels. Each of these gels exhibited similar gelatin behaviors in the temperature range of -10 to 50℃. The gelling time ranged from 20 min to 4 h. With the increase of temperature from -5℃ to 50℃, higher (35℃ to 50℃) or lower (-5℃ to 10℃) temperatures facilitated the ultimate formation of the gel into a three-dimensional porous network structure. The formation of the structure depends on the intertwining, overlap and adsorption between the distinctive molecular chains. A higher HA content resulted in a shorter gelling time. For example, the gelling time for Gel1 (2% of HA) was 6 min, while for Gel2 (1% of HA), Gel3 (0.5% of HA) and Gel4 (0.1% of HA), it was 10 min, 12 min and 25 min at 37℃, respectively. The various monomers and compositions allow for the synthesis of unique copolymers. HA-based materials offer great

advantages including biocompatibility and versatility in producing materials with a considerable range of properties. One of the important characteristics of the ideal scaffold materials is its temperature-sensitive property. The gels can be easily optimized to prepare softer gels using different reaction systems (e.g., by reducing the concentration of the monomers in the solution) or using different reaction methods (e.g., the film plays a critical role in the sol-gel transition). Moreover, the results of this study had important implications for the recent interpretation that the effect of temperature on the gelling process, such as the gelling time, was a recognizable factor for the degree of temperature sensitive. Therefore, the CCAG hydrogels exhibited rapid gelation in the temperature range of 36-37℃with a nearly complete sol-gel transition within 10 min.

Swelling ratio analysis

To develop materials with less side biological effects caused by the adsorption and desorption of body fluids, it is necessary to identify which process is adopted, and if so, whether the process is reversible. PBS and physiological saline with various pH values were adopted as swelling media to mimic the body fluids to study the swelling-shrinking process of the hydrogel when we place it into body fluids. As observed in Fig. 5(1), the swelling ratio of the hydrogels in acidic or basic solution is usually higher than that in neutral solution because some functional groups of the hydrogels can be protonated or ionized in acidic or basic conditions. The in situ adsorption may be more relevant to the application of these materials as fillers injected into subcutaneous tissues in vivo. However, the swelling or deswelling of the hydrogels after immersion in medium is important for understanding the relationship between the winding, tightening, unlocking, and expanding of chains and the temperature or pH. The expansion and shrinkage of the CCAG hydrogels were dependent on the relationship between the correlation of the water molecules and the hydrophilic-hydrophobic group and their intrinsic ionic group (-CONH, and $-NRH_2^+$), which have different degrees of ionization. A similar result was observed for the PNIPAAm hydrogel, as reported by Li et al.[34]

The CCAG hydrogel was divided into [X] and [Y], containing the hydrophobic block and hydrophilic block (see Table. 3A). As observed in Fig. 5(1), at temperatures lower than 35℃, the hydrophilic groups were bound with water molecules via hydrogen bonding, which played a critical role in the swelling process. At higher temperatures from 35℃ to 37℃, the hydrogen bonds became weaker, and the role of the hydrophilic group was decreased. At temperatures above 37℃, the motion of the water molecules was increased, which disrupted the hydrogen bonds and strengthened the interaction between the hydrophobic groups. In the CCAG hydrogels (see Table 3A), -CONH of HLC does not ionize or accept a proton,[29] while -CONH of the side chains (HLC chains) is easily broken into $-COO^-$ and $-NH_3^+$ in basic or acidic solution.[34] In acidic conditions, $-NH_2$ does accept a proton and becomes $-NH_3^+$. In basic conditions, $-NRH_2^+$ and -COOH were ionized and became –NRH and $-COO^-$. When the electric charges of CCAG hydrogels became electrically neutral, attractions between the opposite charges were larger than the repulsion between the same charges, leading to a state of shrinkage. The difference between the number of positive and negative charges led to a net charge, the increased repulsion of opposite charges and a state of gradual expansion.

From the reasons discussed above, we could infer that the swelling ratio of the CCAG hydrogel is dependent on pH (ranging from acidic to basic) and temperature (ranging from 20 to 60℃). Table 3B demonstrates a "shrink-thermo-shrink" feature in acidic condition at temperatures ranging from 20 to 60℃, which is proved by the data in Fig. 5(1-A). The swelling ratio of the CCAG hydrogels increased to the maximum value at 35℃. The chains were expanded to a maximum, and a large number of media could flow into the pores of the hydrogels. Table 3B reveals a "thermo- equilibrium swelling" feature in neutral condition, the evidence of which was also observed in Fig. 5(1-B). When the temperature was as high as 37℃, the swelling ratio was not changed completely, and the swelling equilibrium was exhibited. Fig. 5(1-D) is also consistent with the phenomenon of Table 3B, revealing a "shrink-thermo-shrink" feature in basic conditions. From Table 3B, the characteristic of the swelling ratio of the CCAG hydrogels also revealed that the swelling ratio of the hydrogels in basic media was higher than that in acidic media, while the lowest swelling ratio appeared in neutral media. Fig. 5(1-C) is also consistent with the above conclusions. Thus, the swelling behaviors of the CCAG hydrogels were dependent on the water molecules, hydrophobic-hydrophilic interaction and the electrostatic interaction of the hydrogels.

Baker et al.[35] suggested that the strong dependence of the swelling behavior of acrylamide hydrogels on the initial monomer concentrations was a reflection of increasing network-chain interpenetration with increasing monomer concentration. The swelling behaviors of natural synthetic hydrogels were also similar. With increased HA content, the absorption of hydrogels gradually increased. Therefore, Gel1 resulted in a higher equilibrium water content or swelling ratio whether in acidic, neutral or basic medium. For example, the swelling ratio of Gel1 was higher than that of the other hydrogels (Gel2, Gel3 and Gel4) at various temperatures and in various media (Fig. 5(1)). Therefore, the CCAG hydrogel is pH/temperature sensitive.

In Fig.5(2), when the CCAG hydrogels were soaked, the porous structure became collapsed (see A-B-C) or shrunken (see C-D) due to the surface tension of water pulling the polymer chains together during the wetting process. To avoid this problem, water inside the CCAG hydrogels was replaced with physiological saline and PBS (pH=7.4), which was similar to body fluids, prevented the porous structure from collapsing, eventually yielded the desired equilibrium swelling ratio (see A-E-F). One of the unique properties of CCAG hydrogels is that the gels are highly elastic in the swollen state (A-B-C or A-E). Compared with conventional CS/β-Gp hydrogels[25], the CCAG hydrogels were not easily broken when compressed. The elastic and rubbery properties made CCAG hydrogels

candidates for various applications where resilient gels were preferred. The resiliency of the full water-swollen CCAG hydrogels has never previously been observed. Elastic water-swollen CCAG hydrogels can resist various types of stresses, including tension, compression, bending and twisting.

Table 3. The swelling or shrinking of the CCAG hydrogels depends on the hydrophobic-hydrophilic interaction and the electrostatic interaction in various media: (A) pH sensitivity and (B) temperature sensitivity.

(A) CCAG hydrogel	[X] and [Y]	The pH-sensitive group of Hydrophobic/Hydrophilic Long Blocks	The pH-sensitive group in different media		
			acidic	neutral	basic
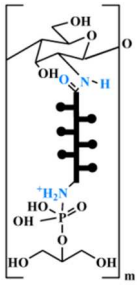	[X]	Hydrophobic Long Blocks (-RNH_2^+, -COOH,-NH_2)	-RNH_2^+ -COOH -NH_3^+	-RNH_2^+ -COO^- -NH_3^+	-RNH, -COO^- -NH_2
		Hydrophilic Long Blocks (-COOH,-NH_2)	-COOH -NH_3^+	-COO^- -NH_3^+	-COO^- -NH_2
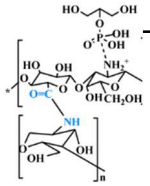	[Y]	Hydrophobic Long Blocks , (-RNH_2^+, -COOH,-NH_2)	-RNH_2^+ -COOH -NH_3^+	-RNH_2^+ -COO^- -NH_3^+	-RNH -COO^- -NH_2

(B) Temperature (℃)	Long blocks of the action at different temperature	Number of charges in the protonated at different media		
		acidic	neutral	basic
T<35℃	Hydrophilic Long Blocks	1 (+)	0	1 (-)
35℃<T<37℃	Hydrophobic/Hydrophilic Long Blocks	5 (+)	2 (+)	3 (-)
T>37℃	Hydrophobic Long Blocks	4 (+)	2 (+)	2 (-)

Structure of hydrogels

The morphology of the lyophilized CCAG hydrogels was examined by SEM, which revealed that the structure of the hydrogels changes from nonporous to microporous and the hole wall changes from thin to thick with different concentrations of HA throughout the cross-section and vertical-section (Fig. 6A). For β-Gp, the gel formation depended on the CCA chains, and an interconnectivity among pores was observed, which is likely due to the cross-linking effects between the phosphate group and -P=O through a reaction with protonated -NH_3^+ in the end chain of HLC to a new chemical bond -RNH_2^+ (as discussed previously). For a higher concentration of HA, the CCAG hydrogels did not exhibit a uniform microporous structure and exhibited poor pore interconnectivity (Fig. 6A, cross-section and vertical-section of Gel1). For a lower concentration of HA, the CCAG hydrogels exhibited a uniform microporous network, indicating good interaction between the components (Fig. 6A, cross-section and vertical-section of Gel3 and Gel4). However, for Gel2, the morphology of the cross-section and vertical-section consisted of a rougher structure. The bulk structure of the hydrogel cross-section confirmed the diffusion of the CCA polymers inside the hydrogels, possibly forming the initial phase of multilayer growth inside the intrinsic pores due to the negatively charged HA. However, CCA chains diffusion inside of the pores can affect the swelling properties of the resultant CCAG hydrogels. We observed that the CCAG hydrogels exhibited a significant change in the liquidity of the water molecules with various pore sizes, while there was no significant effect of the number of layers on the swelling behavior. This result suggests that the observed changes in pore size may be due to the HA modification of only the structure of the hydrogels with a more pronounced effect on the bulk hydrogel properties.

***In vitro* enzyme degradation behavior**

In vitro degradation of the CCAG hydrogels was conducted at 37℃ for up to 6 weeks treated by collagenase I, HAse and trypsin. The changes in the weight, thickness and morphology with the degradation were also measured. The morphology change of the porous CCAG hydrogels in the presence of the enzymatic was observed by SEM, as shown in Fig. 6A. After a 6-week degradation in the presence of collagenase I, HAse and trypsin, Gel1, Gel2, Gel3 and Gel4 exhibited irregular microporous networks and poor pore interconnectivity, and the hole wall changed from thick to thin on the surface.

After degradation by HAse, the hydrogels exhibited a rough and disorder pore size for all four hydrogel formulations. Moreover, pores were observed on the surface and even on the hole wall, which became thin during degradation. However, no pores were present in the hole wall, and numerous hole walls were cracked or even broken into pieces, leading to many pieces of residues remaining on the surface after the degradation by collagenase I. In contrast, small pieces of residue were observed and even covered the surface and compact porous structures appeared unclear compared with initially during the trypsin degradation.

Fig. 6B illustrates the weight loss of Gel1 versus its immersion time in the absence of collagenase I, HAse and trypsin. As observed in Fig. 6B, Gel1 had very slow degradation rates in collagenase I, HAse and trypsin with significant differences in the degradation behaviors. The addition of collagenase I

significantly accelerated the degradation of the CCAG hydrogels, which caused a decrease in the molecular weight and a change in the degradation behaviors. We measured the weight loss of Gel1 to further explain the degradation mechanism by collagenase I, HAse and trypsin. The degradation of the CCAG hydrogels consists of two stages. In the first stage, the molecular weight of the CCAG hydrogels decreased continuously with the degradation time, and significant weight loss occurred. In the second stage, the molecular weight of the CCAG hydrogels decreased to a low value and experienced little weight loss. After 2 weeks of incubation in enzymes, Gel1 exhibited 12.89% weight loss in the presence of HAse, 7.32% weight loss in the presence of trypsin, and 23% weight loss in the presence of collagenase I (Fig. 6B). After 3 weeks, Gel1 exhibited rapid weight loss with degradation time. Especially in the presence of collagenase I, the weight loss could reach over 25%, while the weight loss only reached approximately 15% in the presence of HAse and trypsin degradation. Under the same conditions, Gel1 lost 30%, 20.41% and 20.5% of its initial weight in 6 weeks in the presence of collagenase I, HAse and trypsin, respectively. In contrast to the degradation of the CCAG hydrogels, the CCG hydrogels reported by Li et al.[10] degraded by collagenase I and HAse lost 30% and 50% of their initial weight, respectively, after 6 weeks. Therefore, the rate of degradation of the CCAG hydrogels was lower than that of the CCG hydrogels, in contrast to the *in vitro* degradation rates. As expected, the rates of degradation of the CCAG hydrogels were significantly enhanced in the presence of HAse, collagenase I and trypsin. In addition, the CCAG hydrogels had a highly porous structure, and less weight loss after degradation occurred with HAse and trypsin compared with collagenase I.

The *in-vitro* degradation of hydrogel systems can be affected by various factors such as the chemical structure, molecular mass, formulation, morphology, and thickness of the used specimen.[36] Increased attention is currently paid to residual hydrogels obtained via the restriction enzyme site by enzyme degradation. The restriction enzyme site of collagenase I is the peptide hydroxyproline–Leu–Gly–Pro–Ala in the molecular chain of the collagen;[10] the restriction enzyme site of HAse is β-1,4-glycosidic bond between the D-glucuronic acid residues and N-acetyl-β-D-glucose; and the restriction enzyme site of trypsin is Arg(Lys)-//-X, the peptide bond lying on the carboxy terminus of arginine and lysine. According to the above weight loss dates and SEM images before and after degradation, the mechanism of degradation occurs as illustrated in Scheme 2. The CCAG hydrogels were composed of HLC, CS, HA and β-Gp. After HAse degradation, the CCAG hydrogels broke up into A, B and C by cutting off the restriction enzyme site 1 and 2. As the CCAG hydrogels were combined with the restriction enzyme site of collagenase I, the chains of the hydrogel were cut into D and E from site 3. For trypsin, it is the restriction enzyme site from site 4 of the CCAG hydrogels chains. Therefore, the chain could be divided into F and G. According to the restriction enzyme site and the residues of degradation, we could infer that the molecular weight was decreased.

Characteristics of hydrogels in mice

In most situations, degradation is undesirable because the device is intended to remain in the body for a long period without any change in its functional properties and without inducing any significant adverse response from the tissues.[37] All the experiments were performed in compliance with the relevant laws and institutional guidelines. Approximately 200 μl of the block copolymer solution was injected subcutaneously into Kunming mice. The sol formed a round or regular shaped skin protrusion (Fig. 7A). The hydrogel was not degraded until 6 weeks (Fig. 7C). The mice were sacrificed 10 min after injection, and the hydrogels and tissue were removed from the mice (Fig. 7D). Then, the injected hydrogels could easily be removed (enucleated) from their capsules as a discrete entity using surgical scissors and tweezers. The hydrogels exhibited a transparent, jelly-like appearance (Fig. 7E). The appearance and shape of the CCAG hydrogels (Fig. 7 E and F) obtained from the tissue (Fig. 107) and test tube (Fig. 7G) were similar. In addition, the identical phenomenon in Fig. 7E and Fig. 7F indicated that the gelling time of the CCAG hydrogels is 10 min at 37℃. The results indicated that the sol-gel transition was rapid and that the hydrogel was well suited to both the pH and temperature of the tissue fluid surrounding the site.

TEM analysis

The *in vivo* histocompatibility[10] of the hydrogels was investigated by TEM analysis, and the results were compared with a control group (Fig. 8). The control group was characterized by scattered collagen fibers, visible macrophages, neutrophils and a small amount of cell soma. However, 6 weeks after injection, the appearance of the collagen fibers changed from sparse to scattered (Fig. 8 A, B and C).

After the injection of Gel1, a large number of macrophages, inflammatory cells and collagen fibers were observed. At week 1, the macrophages began to lose their cylindrical shape, whereas the engulfed foreign body did not appear (Fig. 8D). At week 2, the collagen fibers maintained their initial shape; however, macrophages and inflammatory cells on their tissue had become more numerous. At week 6, the collagen and macrophages appeared as they had at week 2, while the residues after degradation were slightly more abundant than the cell soma in the tissue (Fig. 8 D, E and F).

At weeks 1, 2 and 6, there was a typical inflammatory response at the site of injection of Gel2 (Fig. 8 G, H and I). Collagen fibers, morphology and lipid droplets were plentiful adjacent to the injection site. At the tissue site, there was an irregular shape of macrophages encircling the collagen fibers and a large number of lipid droplets surrounding the cytoplasm. The density of the collagen fibers and lipid droplets increased slightly at week 2 and remained almost unaltered thereafter during the 6 weeks of investigation.

However, there was a typical biological response at the site of the injection of Gel3, similar to the control group. After the injection of Gel3 at week 1, a large number of dense collagen fibers scattered each other, appearing first at the periphery of

the tissue. Six weeks following the injection, the full sparse of the collagen fibers were occupied by collagen matrix with only a few cell somas present (Fig. 8 K and L).

Furthermore, the injection of Gel4 led to an increase in the number of collagen fibers and cells including macrophages, fibroblasts and fibrocytes (Fig. 8 M). Two and six weeks after injection, it was observed that the collagen fibers were transverse and longitudinal crossed and that the amount of phagocytic cells and capillaries decreased with the injection time (Fig. 8 N, O).

From comparison with reports by Li et al.,[10] the tissue reaction to the CCAG hydrogels was different from that of the CCG hydrogels. For the CCG hydrogels, a large number of macrophages lymphocytes, and fibroblasts surrounded the injection site, and collagen fibers, lysosomes and lipid droplets were observable adjacent to the tissue site. For the CCAG hydrogels, less macrophage surrounded the injection site, while the collagen fibers and lipid droplets were also observable in the areas surrounding the injection site. It was concluded that the HA concentration is the key factor affecting the histocompatibility of the hydrogels and even decreased the inflammatory reaction after injection. The degree of inflammation reaction caused by Gel3 was small and gradually disappeared over time, and this inflammatory reaction was the same as that of the control group. However, the inflammatory reaction from Gel1, Gel2 and Gel4 did not decrease with time and exhibited a significant difference from the control group. Therefore, Gel3 exhibited the lowest limitation of inflammatory reaction and exhibited good histocompatibility. As fibrous films are one of the components of hydrogels their existence and function will play an important role in filling tissue, which is mainly because the materials, as substitutes for tissue, will gradually adapt to the surroundings of the tissue and even become one part of the tissue intrinsically.

Immunohistochemical staining of skin tissue by CD68

To investigate the biological response to the injected CCAG hydrogels, the tissue surrounding the hydrogels was evaluated histologically after staining with CD68. From TEM analysis, macrophages exist mainly for the inflammatory cell. Here, we studied the macrophages as measures of the effectiveness of the histocompatibility. Immunohistochemical staining of the skin tissue with anti-CD68 mAb revealed that the distribution of CD68 was mainly in the hydrogels, subcutaneous tissue, hair follicles, pigment cells and fat cells at 1, 2 and 6 weeks (Fig. 9). However, there was no staining of sweat pores, sweat ducts, erector muscles, eccrine sweat glands, hair bulbs or apocrine sweat glands. At the gel-tissue interface, there was a thin capsule containing macrophage-like or fibroblast-like cells encircling the gels or tissue. As reported by Li et al.,[10] one concern was that the excessive stain of the hydrogels would impair the biocompatibility of the CCAG hydrogels. Furthermore, the depth of color has very potent effects that include immunoreactivity and inflammatory responses. Therefore, stain minimization was important to be able to provide local anti-inflammatory activity while minimizing systemic effects or the dehiscence of nearby wounds. It was observed that the hydrogels and tissue were intensively stained. Even with this very long injection, the degree of stain decreased or disappeared mainly on the hydrogels and hair follicles; however, the pigment cells and fat cells were shown positively. Conversely, the importance of these considerations regarding stain was confirmed by the mildly increased positivity of Gel1 and Gel2 compared with Gel3 and Gel4 at week 6. Therefore, the Gel3 and Gel4 have less inflammatory responses.

H&E analysis

Numerous investigators have reported the effectiveness of ideal materials for filling tissue in preventing the excessive degradation of hydrogels. These hydrogels are reported to act, among other mechanisms, by reducing the production of foreign bodies by macrophage cells and fibroblast cells without degrading the hydrogels and periphery tissue. The histological response and degradation behaviors after the injection of the hydrogels at 1, 2 and 6 weeks were analyzed by H&E staining (Fig. 10). Upon injection, the hydrogels degraded gradually with time *in vivo*; however, the degradation behaviors of Gel1, Gel2, Gel3 and Gel4 were different. The degradation behavior of the hydrogels could be changed using many approaches. The three-dimensional (3D) mesh structure of the hydrogels could be modified by altering the cross-linking density of the sol (the concentration of the fibers with different contents of HA) and the nature of the cross-link between HLC, HA and CS. Altering the rate of hydrogel degradation could also affect the structure of the hydrogels after being injected into tissue. Furthermore, we observed no adverse effects from the cross-linked HA in this study or others[38,39] because of its potency such that it would be possible to achieve a given anti-inflammatory effect with the least possible alteration of the biologically benign shape after injection. In particular, we wished to avoid rendering it deformed. When hydrogels were injected into subcutaneous tissue, the body fluid could flow into the hydrogel pores and transport nutrients and water to tissue. The degradation behaviors include three steps: degradation from the interspaces, multilayer and periphery of the hydrogels. The direction is mainly dependent on the structure of the hydrogels.

From Fig. 10, Gel1 exhibited a complete structure and shape. Only the size decreased, and the internal structure has a split of gap after 6 weeks. Gel2 was degraded, and the shape was changed, with a larger gap appearing at 2 and 6 weeks. The shape of Gel3 appears to not be changed entirely; however, some larger residual fragments of hydrogels remain in the tissue. For Gel4, only a small portion of residual debris of the hydrogels remains in the tissue. The structure of the hydrogels has been changed entirely.

Therefore, Gel3 seemed to cause a lower degradation rate than the other hydrogels used here. It is important to note, given the unique function of HA to hydrogels, that this result could reflect an anti-inflammatory effect rather than a direct anti-degradation effect. The fibers are mixed by HLC, HA and CS, which improve the ability of anti-degradation and the stability of the structure. The body enzyme solution and inflammatory

cells have been tolerated to tissue and decreased the erosion of the hydrogels by inflammatory cells. Furthermore, it is likely that the inflammatory response of un-cross-linked HA[10] would be much higher than those tested here after mixing. In fact, our results indicated that the biocompatibility of CCAG hydrogels is comparable to that of CCG hydrogels and causes an even milder inflammatory response. The CCAG hydrogels may be an ideal injectable body filling material for use as a tissue engineering scaffold for the restoration of wrinkles and tissue cavities formed by surgery.

Conclusions

PH/temperature-sensitive CCAG hydrogels were successfully synthesized by a combination of fibers (CCA) and β-GP by self-assembly. Well-defined fibers were prepared from CS, HLC and HA and subsequently functionalized with an HA monomer. The CCAG hydrogels exhibited rapid gelation in the temperature range of 36-37℃ at neutral pH with a nearly complete sol-gel transition within 10 min after being subcutaneously injected into Kunming mice or placed in a test tube under 37℃. The introduction of a new amide bond (-CONH) and -NRH_2^+ into the polymerizable groups resulted in a "shrink-thermo-shrink" or "thermo-equilibrium swelling" feature from the cross-linked network under mild conditions. The water molecules, hydrophobic-hydrophilic interaction and the electrostatic interaction of the hydrogels had minimal effects on the swelling equilibrium, suggesting that the equilibrium temperature was 37℃ in physiological saline or PBS (pH 7.4). The swelling ratio was decreased at a lower proportion of HA in various media. Furthermore, the CCAG hydrogel had a highly porous structure, which would provide more space for water and small molecules to move freely in the network. Additionally, the chemical structure and molecular mass, formulation, morphology, and the thickness of the hydrogels significantly affected the *in-vitro* degradation of the hydrogel systems. The results indicated that the CCAG hydrogels had a highly porous structure and the lowest weight loss after degradation by HAse and trypsin compared with collagenase I. *In-vivo* assays suggest that these CCAG hydrogels are histocompatible and that the introduction of HA into fibers promoted the anti-inflammation, anti-degradation and stability of the structure of the CCAG hydrogels. For example, Gel3 (0.5% HA) triggered no adverse effects compared with the control group (the parameters including the morphology of the cell, the species of cell and the quantity of cell), showed negative staining after immunohistochemical staining of skin tissue by CD68, was resistant to morphological change, and was degraded slowly after H&E staining. Consequently, these fibers by self-assembly appear to be promising for tissue engineering applications, enabling control over the properties of hydrogels including gelling time, swelling ratio, and degradation *in vitro* and *in vivo*. In summary, the CCAG hydrogel was proven to be highly suitable as an injectable body filling material as well as a tissue engineering scaffold for the restoration of wrinkles and tissue cavities formed by surgery.

Acknowledgements

This study was financially supported by the National Natural Science Foundation of China (21276210, 21106112, 21206135, 31000019 and 21106111) and the NWU Graduate Innovation and Creativity Funds (YZZ12037) and the Shaanxi Key Subject Program, China.

Notes and references

Shaanxi Key Laboratory of Degradable Biomedical Materials, Department of Chemical Engineering, Northwest University, Taibai North Road 229, Xi'an, Shaanxi 710069, China
** Corresponding author: Tel.: +86- 29-88305118; Fax: +86-29-88322585*
E-mail address: fandaidi@nwu.edu.cn (D. D. Fan)

Abbreviations

CS: chitosan
HAc: acetic acid
HLC: human-like collagen
HA: hyaluronic acid
β-GP: β-sodium glycerophosphate
PBS: Phosphate buffered saline
CCA: CS-HLC-HA
CCG: CS-HLC/β-GP
CCAG: CS-HLC-HA/β-GP
HAse: Hyaluronidase
FT-IR: Fourier transforms infrared spectroscopy
XPS: X-ray photoelectron spectroscopy
SEM: scanning electron microscopy
TEM: transmission electron microscopy
H&E: hematoxylin and eosin
LBL: Layer-by-layer

1 I. R. Degano, L. Quintana, M. Vilalta, D. Horna, N. Rubio, S. Borros, et al., *Biomaterials*., 2009, 30, 1156-1162.
2 J. M. Lehn, *Science*., 2002, 295, 2400-2403.
3 C. A. E. Hauser, S. G. Zhang, *Chem. Soc. Rev*., 2010, 39, 2780—2790.
4 G. Decher, *Science.*, 1997, 277(5330), 1232 – 1237.
5 D. L. Elbert, C. B. Herbert, *J. A. Hubbell. Langmuir*., 1999, 15(16), 5355–5362.
6 S. Y. Yang, J. D. Mendelsohn, M. F. Rubner, *Biomacromolecules.*, 2003, 4(4), 987–94.
7 J. D. Mendelsohn, S. Y. Yang, J. Hiller, A. I. Hochbaum, M. F. Rubner, *Biomacromolecules*., 2003, 4(1), 96–106.
8 T. Huaping, R. Constance, *Biomaterials*., 2009, 30, 2499-2506.
9 Y. Seda, S. Shilpa, B. D, Thomas, *Biomaterials*., 2011, 32, 5590-5599.
10 A. J. DeFail, C. R. Chu, N, Izzo, K, G, Marra, *Biomaterials*., 2006, 27, 1579–1585.
11 A. Oswaldo. E. W. Lozoya, A. Rachael, *Biomaterials.*, 2011, 32, 7389-7402.
12 B. J. Leacha, E. S. Christine, *Biomaterials*., 2005, 26, 125–135.
13 L. Richert, P. Lavalle, E. Payan, X. Z. Shu, G. D. Prestwich, J. F. Stoltz, et al., *Langmuir*., 2004, 20(2), 448–458.

14 X. Li, X. X. Ma, D. D. Fan, C. H. Zhu, *Soft Matter*., 2012, 8, 3781-3790.
15 Y. Zhai, F. Z. Cui, and Y. Wang, *Current Applied Physics*., 2005, 5, 429-432.
16 Y. Wang, F. Z. Cui, Y. Zha, X. M. Wang, X. D. Kong, and D. D. Fan, *Materials Science and Engineering C*., 2006, 26, 635-638.
17 Y. Zhai, and F. Z. Cui, *Journal of Crystal Growth*., 2006, 291, 202-206.
18 C. H. Zhu, D. D. Fan, Z. G. Duan, W. J. Xue, L. A. Shang. et al., *Journal of Biomedical Materials Research Part A*., 2009, 89(A), 829-840.
19 R. R. Costa, C. A. Custõdio, F. J. Arias, J. C. Rodríguez-Cabello, *J. F. Mano, Small*., 2011, 7(18), 2640-2649.
20 K. E. Crompton, J. D. Goud, R. V, *Biomaterials*., 2007, 28, 441–449.
21 T. Y. Guo, Y. Q. Xia, J. Wang, M. D. Song, B. H. Zhang, *Biomaterials*., 2005, 26, 5737–5745.
22 G. Molinaro, J. C. Leroux, J. Damas, A. Adam, *Biomaterials*., 2002, 23, 2717–2722.
23 K. Obara, M. Ishihara, T. Ishizuka, M. Fujita, Y. Ozeki, T. Maehara, et al., *Biomaterials*., 2003, 24, 3437–3444.
24 S. V. Madihally, H. W. T. Matthew, *Biomaterials*., 1999, 20, 1133–1142.
25 L. Casettari, D. Vllasaliu, J. K. W. Lam, *Biomaterials*., 2012, 33, 7565-7583.
26 P. M. Santos, J. G. Winterowd, G. G. Allen, M. A. Bothwell, and E. W. Rubel, *Head and Neck Surgery*., 1991, 105, 12-25.
27 H. J. Chung, D. H. Go, J. W. Bae, I. K. Jung, J. W. Lee, and K. D. Park, *Current Applied Physics*., 2005, 5, 485-488.
28 F. Ganji, M. J. Abdekhodaie, and A. S. A. Ramazani, *Journal of Sol–Gel Science and Technology*., 2007, 42, 47-53.
29 X. Li, D. D. Fan, X. X. Ma, C. H. Zhu, et al., *Soft Materials*., 2014, 12, 1-11.
30 Q. Feng, G. C. Zeng, P. H. Yang, C. X. Wang, *J. Y. Cai, Eng. Aspects*., 2005, 257, 85-88.
31 P. F. Yang, C. K. Lee, *Biochemical Engineering Journal*., 2007, 33, 284-289.
32 H. G. Wu, Z. A. Yao, Y. Y. Liu, J. X. Dun, C. Yu, L. Y. Shi, B. M. Feng, *Chinese Journal of Biomedical Engineering*., 2008, 27, 580-585.
33 J. J. G. Soest, K. Benes, D. Wit, J. F. G. *Vliegenthart, Polymer.*, 1996, 37, 3543.
34 Y. S. Li, Y. Q. Yu, *Chinese Journal of Colloid &polymer*., 2009, 27(4), 9-12.
35 J. P. Baker, L. H. Hong, H. W. Blanch, *J. M. Prausnitz, Macromolecules*., 1994, 27, 1446-1454.
36 S. C. Tjong, J. Z. Bei, *Polym Eng Sci*., 1998, 38:3-8.
37 D. F. Williams, *Clin Mater*., 1992, 10, 9-14.
38 Y. Yeo, C. Highley, E. Bellas, T. Ito, R. Marini, R. Langer, et al., *Biomaterials.*, 2006, 27, 4698–4705.
39 T. C. Ito, I. P. Fraser, Y. Yeo, C. B. Highley, et al., *Biomaterials*., 2007, 28, 1778-1786.

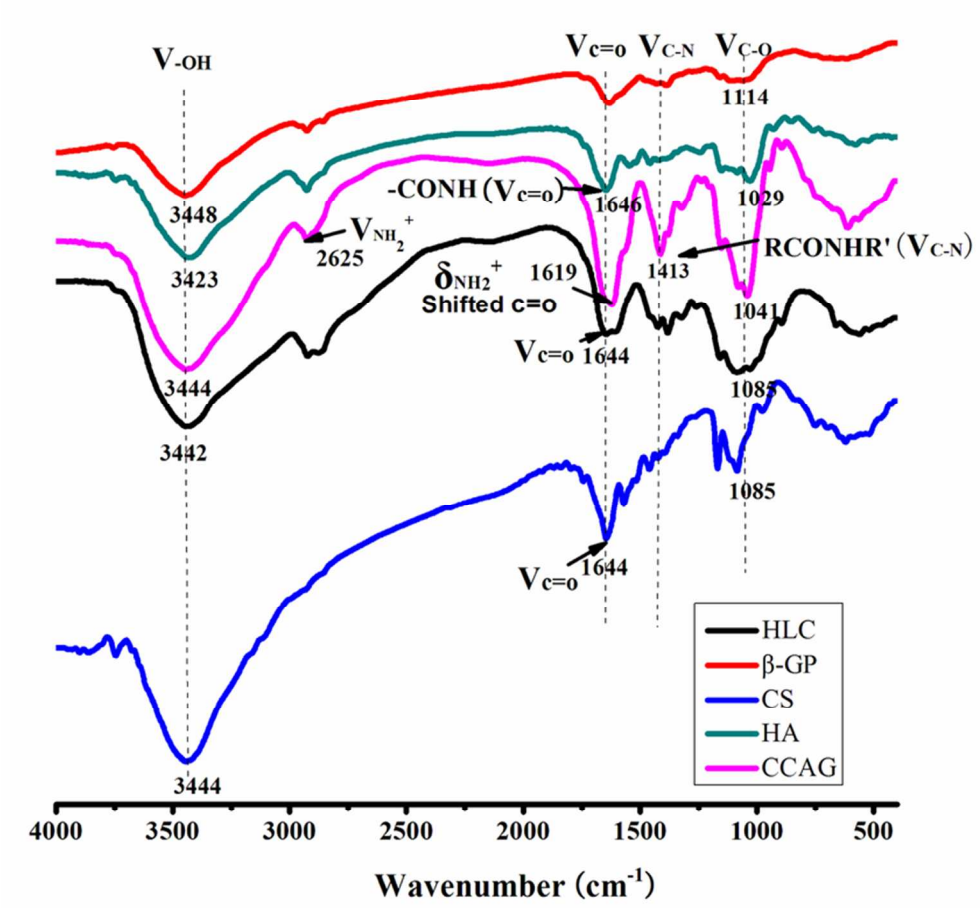

Fig. 1. FT-IR spectra of CS, HLC, HA, β-GP and CS-HLC-HA/β-GP (CCAG) hydrogel.
72x66mm (300 x 300 DPI)

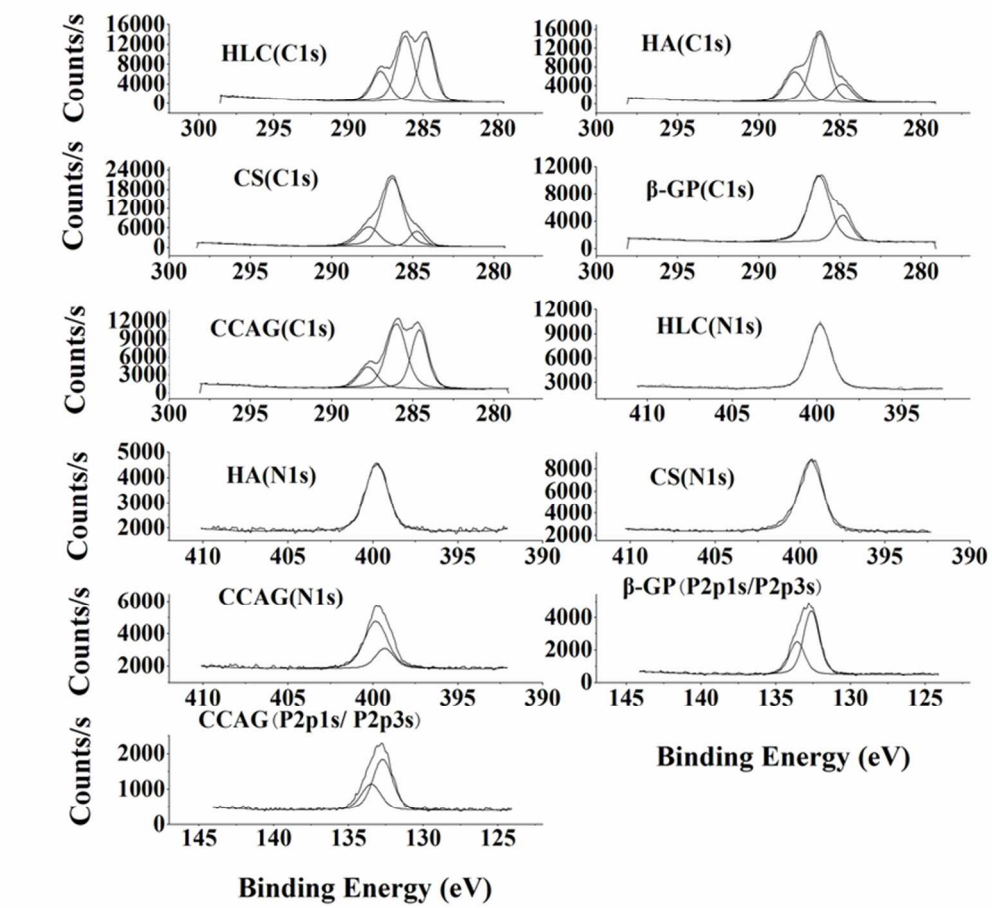

Fig. 2. XPS spectra of CS, HLC, HA, β-GP and CS-HLC-HA/β-GP (CCAG) hydrogel. The C1s, N1s, P2p1, P2p3 spectrum was recorded, respectively.
72x65mm (300 x 300 DPI)

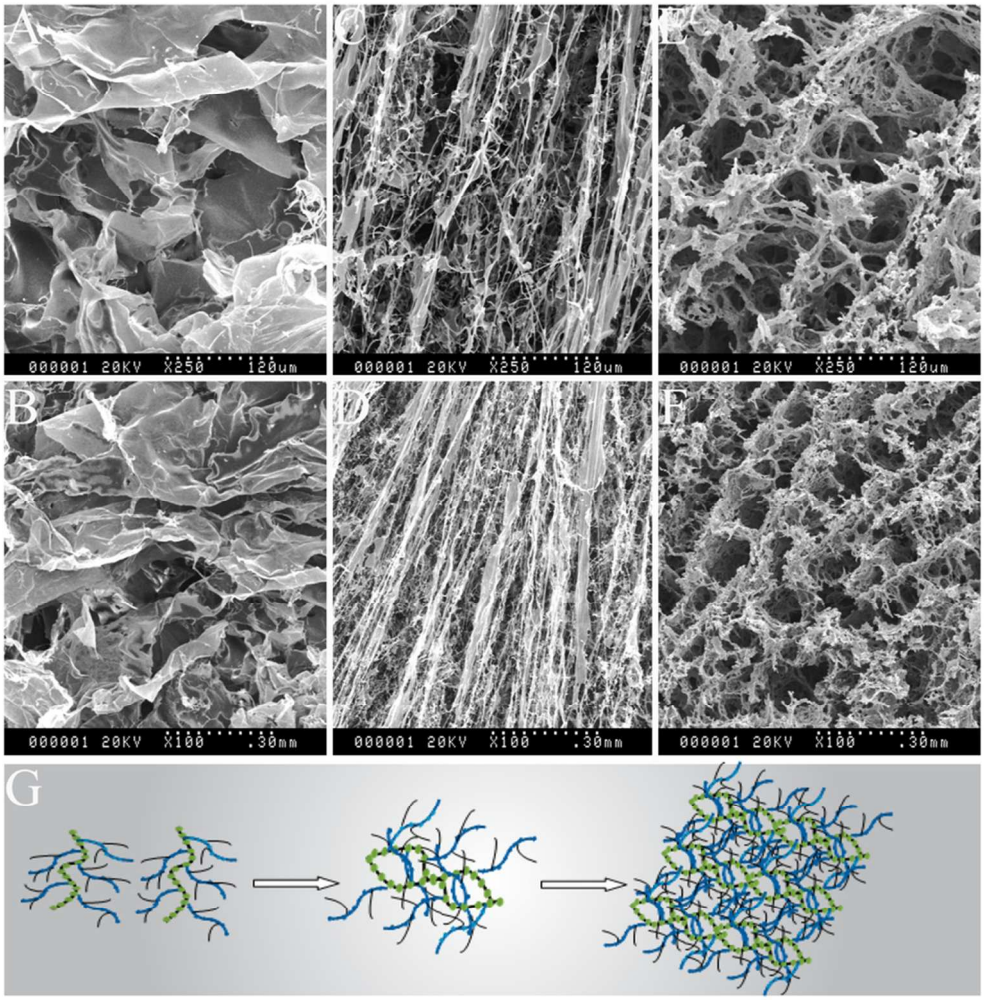

Fig. 3. SEM images (×100, ×250) of CS/HA film (A, B), CS-HLC/HA fibrous chains (C, D) and CCAG hydrogels (E, F); (G) the model of CCA fibrous chains forming process; Scale bar for A, C and E: 30 mm; Scale bar for B, D and F: 120μm.
81x82mm (300 x 300 DPI)

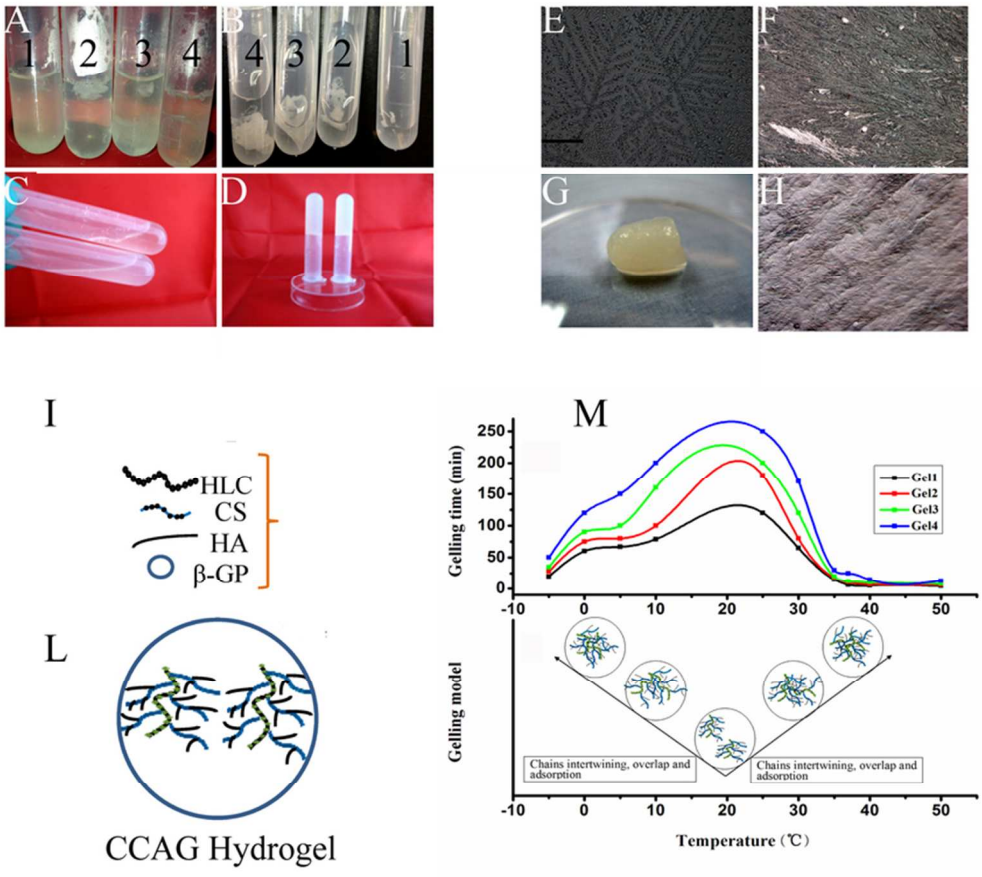

Fig. 4. (A) Visual inspection of the 5% CS mixing with various concentrations of HA (0.1 (1), 0.5% (2), 1% (3) and 2% (4)); (B) the CS/HA films were removed and rinsed with water; (C) visual inspection of the sol at 25℃ for the CCAG solution; (D) the solutions became gels after being placed in a thermo-cell at 37℃; (E) photomicrographs of the single fibrous chain (CS-HLC/0.1%HA); (F) photomicrographs of the fibrous chains (CS-HLC/0.5% HA); (G) the transparent, jelly-like appearance of CCAG hydrogels removed from 10 mL centrifugal tube;. (H) photomicrographs of the fibrous films of (CS-HLC/2% HA); (I) the model of CS, HLC, HA and β-GP; (L) the model of CCAG hydrogel; (H) effects of temperature on the gelling time during the gelatin process; schematic model of the CCAG hydrogel during gelatin process, showing the dependence on temperature. HLC is a main-chain, CS is a sub-chain, and HA is the branched-chain in β-Gp solution. Scale bar for E, F and H: 120 μm.
72x66mm (300 x 300 DPI)

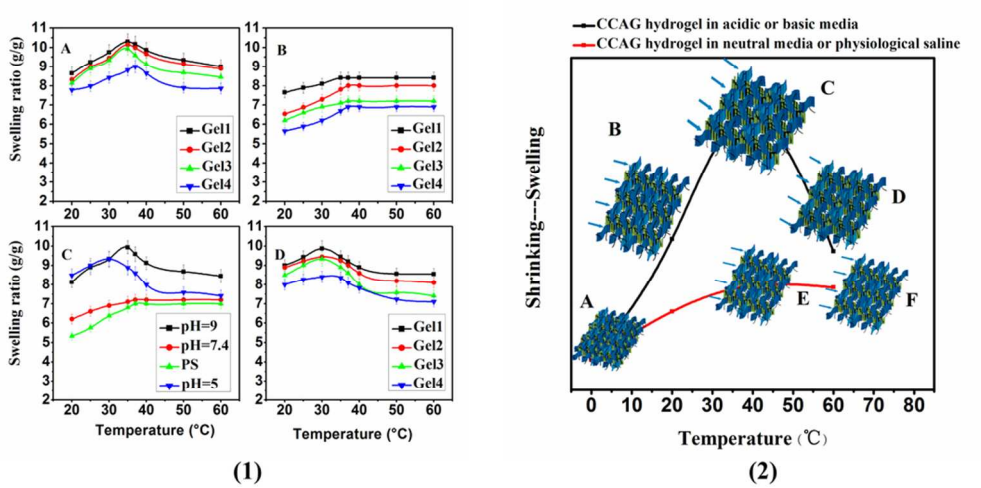

Fig. 5. (1) The swelling ratios of the gels dependence on pH and temperature. A is in PBS (pH=9), B is in PBS (pH=7.4) and D is in PBS (pH=5). C represents the swelling ratio of Gel3 in PBS (9, 7.4 and 5) and physiological saline (PS). (2) The model of the swelling-shrinking of gels in acidic or basic media (A-B-C-D) and in PBS (pH=7.4) or in physiological saline (A-E-F).
91x49mm (300 x 300 DPI)

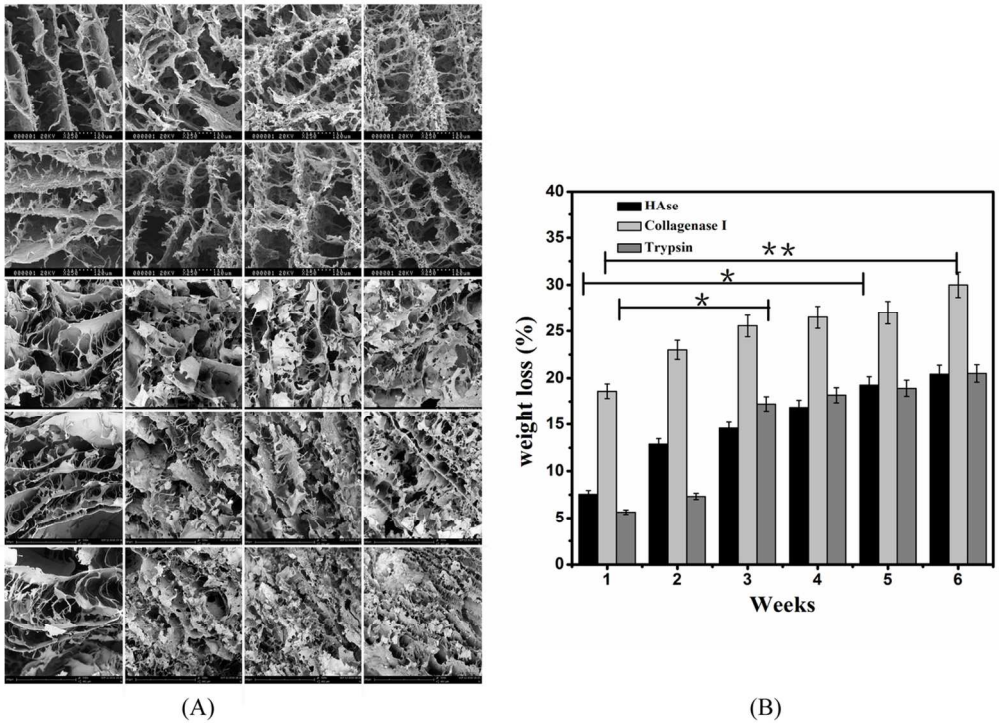

Fig. 6. (A) SEM images (×250) of Gel1, Gel2, Gel3 and Gel4 at 37℃ after lyophilization, Scale bar for cross-section and vertical-section: 120 μm.; SEM images (×500) of Gel1, Gel2, Gel3 and Gel4 after degradation by HAse, collagenase I and trypsin, Scale bar for HAse, collagenase I and trypsin degradation: 240 μm. The first row: cross-section; second row: vertical-section; third row: HAse degradation; fourth row: collagenase I degradation; fifth row: trypsin degradation. The first column: Gel1, second column: Gel2, third column: Gel3, fourth column: Gel4. (B) Weight loss of Gel1 after degradation by hyaluronidase (HAse), trypsin and collagenase I.
58x42mm (600 x 600 DPI)

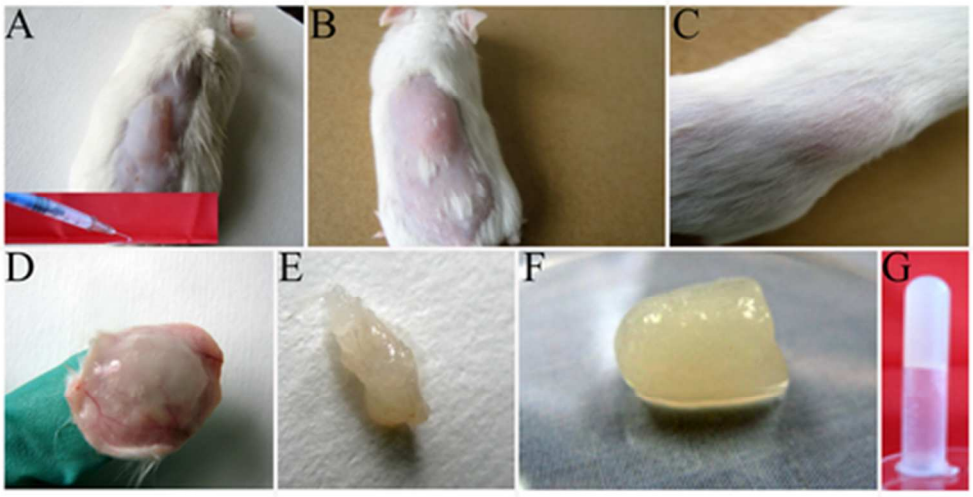

Fig. 7. Approximately 200 μl of the block copolymer solution was subcutaneously injected into Kunming mice. (A) 1 week after injection; (B) 2 weeks after injection; (C) 6 weeks after injection; (D) the mice were sacrificed and the hydrogel and periphery tissue were carefully removed from the Kunming mice after injection using surgical scissors and tweezers; (E) the hydrogels exhibited a transparent, jelly-like appearance after being removed from the mice; (F) the CCAG hydrogel removed from test tube; (G) the CCAG hydrogel in the test tube after being placed in a thermo-cell for 10 min at 37℃. Scale bar for all: 10 mm.
41x21mm (300 x 300 DPI)

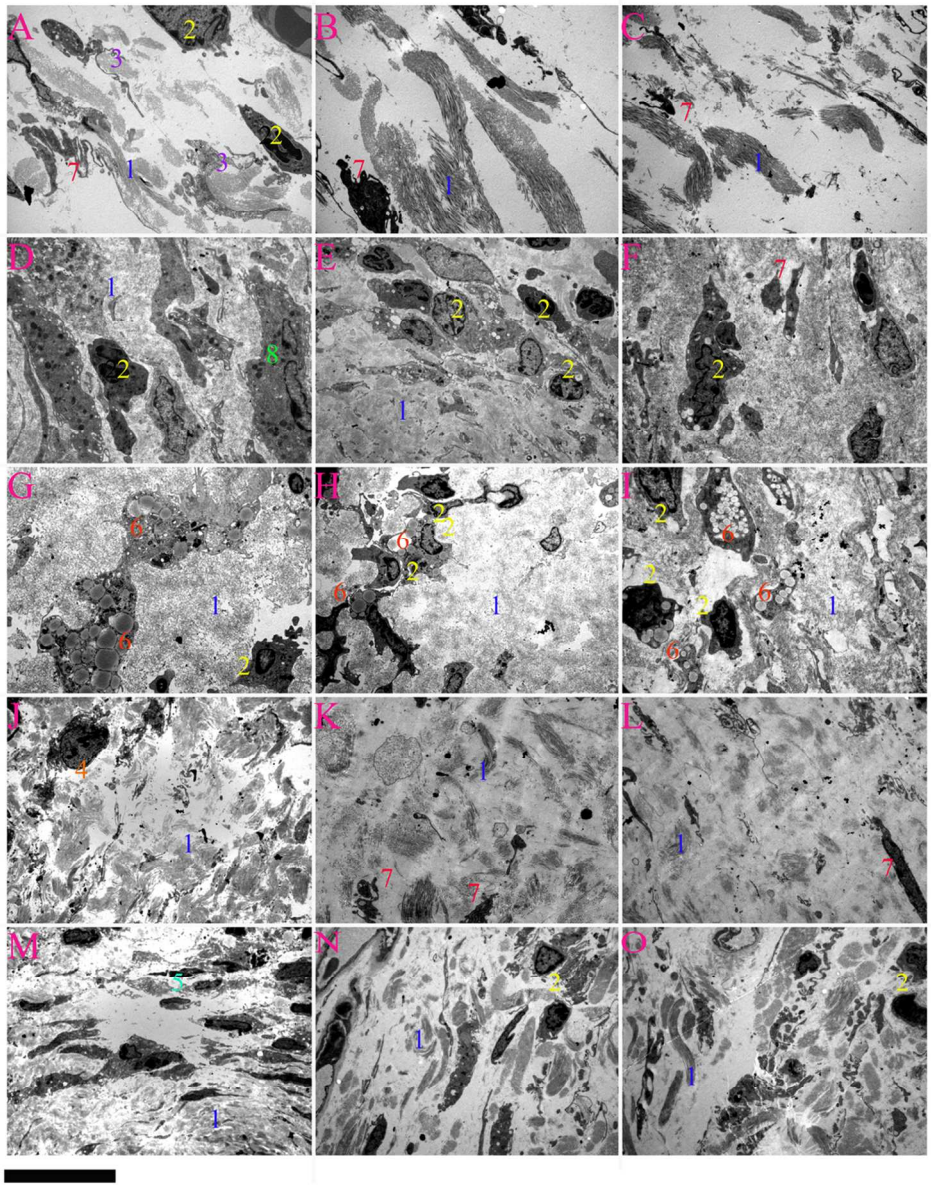

Fig. 8. TEM images at ×3500 magnification of Gel1, Gel2, Gel3 and Gel4 of the site surrounding the tissue, compared with the control group injection with physiological saline. The control group (A, B, C), Gel1 (D, E, F), Gel2 (G, H, I) and Gel3 (J, K, L) and Gel4 (M, N, O). A, D, G, J and M exhibit results 1 week after injection;B, E, H, K and N after 2 weeks; and C, F, I, L and O after 6 weeks. The numbers represent: 1, collagen fibers; 2, macrophages; 3, neutrophilic granulocytes; 4, fibroblasts; 5, fibrocytes; 6, lipid droplets; 7, cell soma; 8, inflammatory cells. Scale bar for all: 20 μm.
102x130mm (300 x 300 DPI)

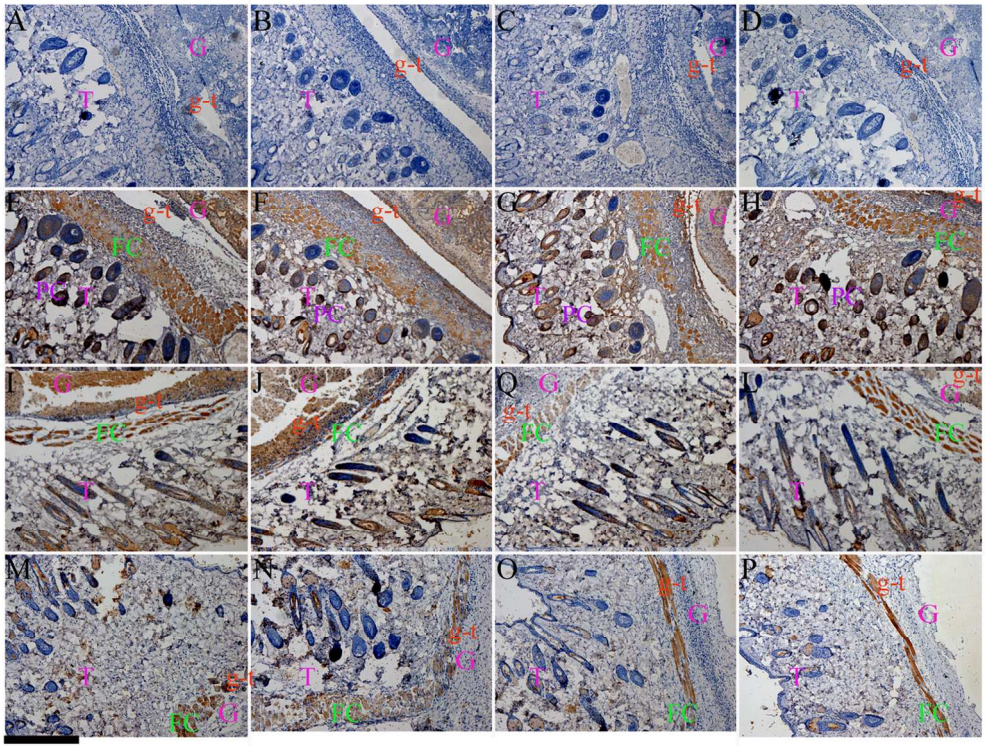

Fig. 9. Images of immunohistochemical staining in mouse tissue for Gel1, Gel2, Gel3, Gel4 and the site surrounding the tissue.Gel1 (A, E, I, M,) Gel2 (B, F, J, N) and Gel3 (C, G, Q, O) and Gel4 (D, H, L, P). A, B, C and D represent the control block one week after injection staining by CD68 without anti-CD68 mAb; E, F, G and H present the results 1 week after injection staining by CD68 with anti-CD68 mAb; I, J, Q and L after 2 weeks staining by CD68 with anti-CD68 mAb; and M, N, O and P after 6 weeks staining by CD68 with anti-CD68 mAb. G represents the hydrogel; T represents the subcutaneous tissue; FC represents the fat cells; PC represents the pigment cells; g-t represents the gel-tissue interfaces. Scale bar for all: 200 μm.
123x92mm (300 x 300 DPI)

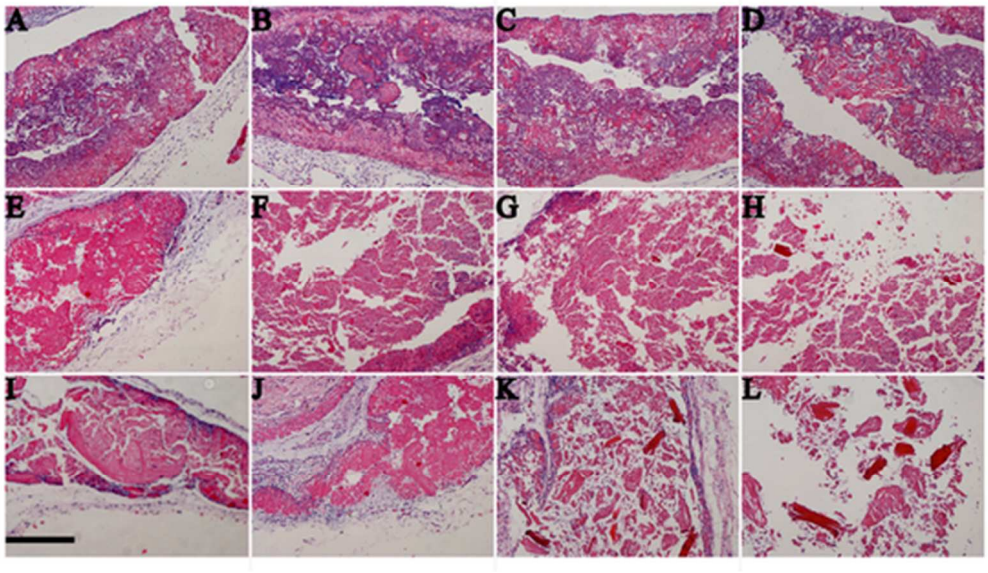

Fig. 10. Photomicrographs of H&E staining for Gel1, Gel2, Gel3 and Gel4 1, 2 and 6 weeks after injection.Gel1 (A, E, I) Gel2 (B, F, J) and Gel3 (C, G, k) and Gel4 (D, H, L). A, B, C and D represent 1 week after injection staining by H&E; E, F, G and H show the results 2 weeks after injection staining by H&E; I, J, K and L show the results after 6 weeks staining by H&E. Scale bar for all: 200 μm.
46x26mm (300 x 300 DPI)

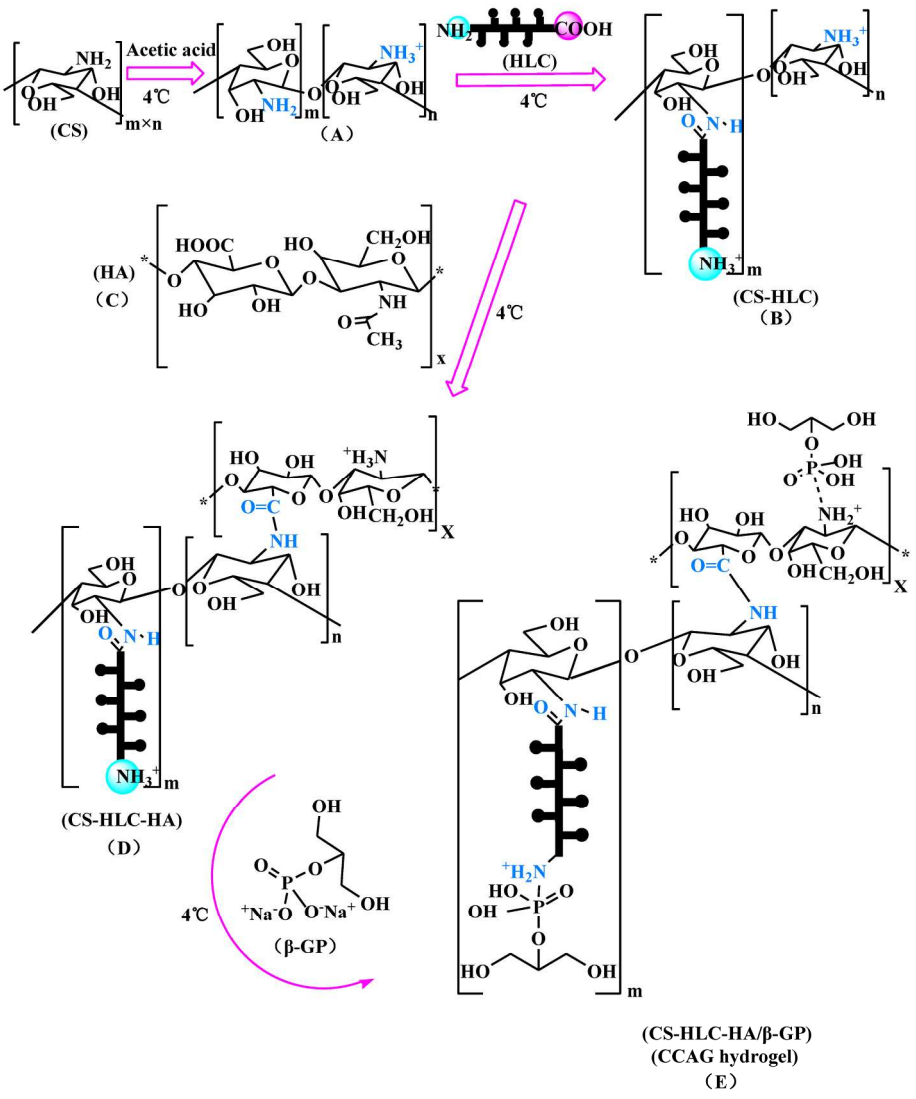

Scheme 1. Proposed mechanisms for the interaction between CS, HLC, HA and β-GP: the protonation of CS in acetic acid solution (A), the reaction between CS and HLC in an ice-water bath (B), HA (C), HA added in CS-HLC solution in an ice-water bath (D), and the CS-HLC-HA fibers added in β-GP to form the CCAG hydrogel (E).
102x131mm (600 x 600 DPI)

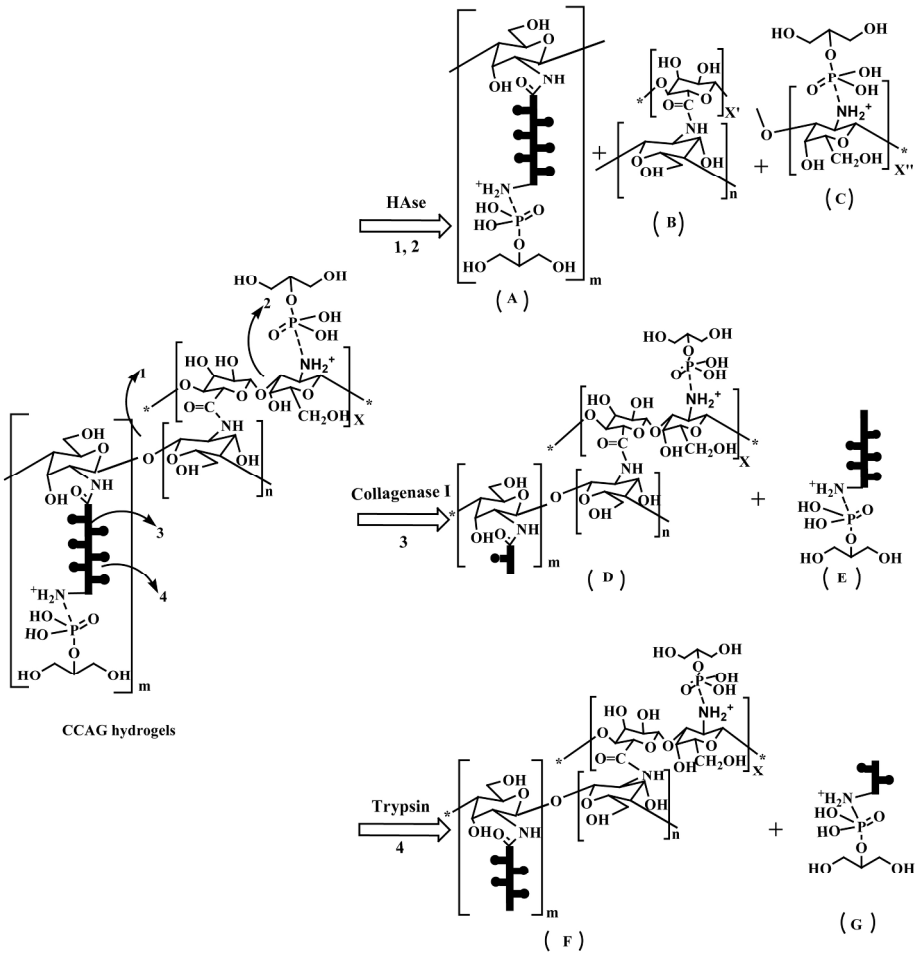

Scheme 2. A schematic of the enzymatic degradation of the CCAG hydrogel in vitro. A, B and C represent the residual hydrogels after degradation by HAse; D and E represent the residual hydrogels after degradation by collagenase I; F and G represent the residual hydrogels after degradation by trypsin. Sites 1 and 2 represent the restriction enzyme site of HAse; Site 3 represents the restriction enzyme site of Collagenase I; and Site 4 represents the restriction enzyme site of trypsin.
242x240mm (300 x 300 DPI)